CARBON 93 (2015) 361–369

Available at www.sciencedirect.com

ScienceDirect

journal homepage: www.elsevier.com/locate/carbon

Controlled synthesis of carbon nanocoils with selective coil diameters and structures by optimizing the thickness of catalyst film

Xin Fu [a], Lujun Pan [a,*], Dawei Li [b], Nan Zhou [a], Yanming Sun [a]

[a] School of Physics and Optoelectronic Technology, Dalian University of Technology, No. 2 Linggong Road, High-District, Dalian 116024, PR China

[b] Department of Electrical and Computer Engineering, University of Nebraska-Lincoln, Lincoln, NE 68588-0511, USA

ARTICLE INFO

Article history:
Received 15 December 2014
Accepted 18 May 2015
Available online 22 May 2015

ABSTRACT

Carbon nanocoils (CNCs) with selective coil diameters and structures have been synthesized by chemical vapor deposition using Sn/Fe binary catalyst films. CNCs, carbon nanofibers and irregular carbon nanowires could be selectively obtained by changing the thickness of the catalyst film. It is found that the coil diameters of CNCs gradually decrease with a decrease in the thickness of the catalyst films within a certain range, indicating that the coil diameters of CNCs can be effectively controlled by adjusting the thickness of Sn/Fe catalyst films. The morphology of the CNCs tends to change from spring-like to plait-like, and the graphitization degree of the CNC increases when their diameters are reduced. Our results provide important guidelines for the controlled synthesis of CNCs with selective coil diameters and selective structures by optimizing the catalyst film thickness.

1. Introduction

Carbon nanocoils (CNCs), a new type of three-dimensional helical nano-material, exhibit outstanding optical, mechanical, and electrical properties [1–6] and have received considerable attention in recent years. Because of these outstanding properties, CNCs are an ideal candidate for a wide range of applications, including electromagnetic wave absorbers [7], micro-sensors [8], and field emission devices [9]. To date, it has been observed that the performance of CNCs is closely linked to their morphology and structure [10–12]. Deng et al. observed that the resonance frequency of a CNC is dependent on its morphology [13]. Ma et al. reported that the resistivity of CNCs decreases with the increase in the annealing temperature, owing to the improvement in the coils' crystallinity [14]. Pan et al. observed that the turn-on voltage of a CNC field emitter is decreased by decreasing the coil diameter of the CNC [15]. Therefore, developing a simple way to synthesize CNCs with controllable coil diameters and structures would be most desirable.

Due to its controllable and simple operation, chemical vapor deposition (CVD) has been widely employed to synthesize CNCs. To date, many metals and their alloys, such as Fe, Cu, Ni, Ti, Co, and Pd [16–19] have been used to grow CNCs, where Fe–Sn–O has proven to be an efficient catalyst and therefore attracted the attention of many researchers.

* *Corresponding author:* Fax: +86 411 84709304.
E-mail address: lpan@dlut.edu.cn (L. Pan).

http://dx.doi.org/10.1016/j.carbon.2015.05.059
0008-6223/

Several methods have been used to prepare Fe–Sn–O catalysts, such as dropping, dipping, or spin-coating a solution of catalyst precursor on substrates; physical evaporation; and sputtering [20–22]. Sputtering is an effective method for obtaining a uniform catalyst film with controllable thickness. In recent years, much work has been done to control the morphology and structure of CNCs. Zheng et al. observed that the reaction temperature greatly affects carbon nanostructures [23]. Liu et al. controlled the morphologies of CNCs by changing the flow rate of acetylene [24]. Li et al. successfully synthesized CNCs with a controlled coil diameter, coil pitch and structure by adjusting the reaction temperature and the delivery of acetylene in a CVD system [25]. In addition, our previous study revealed that the distribution of coil diameters could be altered by increasing the deposition time [26]. It is noted that all of these studies have focused on controlling the morphology of CNCs by changing the reaction conditions in a CVD system or the methods for preparing catalyst particles. The thickness of the catalyst film is also a crucial factor for the growth of CNCs and may affect the size and the distribution of the formed catalyst particles. However, the effects of Sn/Fe catalyst film thickness on the growth and morphology of CNCs have not been adequately investigated.

In this study, we investigated the coil diameter and structure of CNCs growth by monitoring changes in the thickness of Sn/Fe catalyst films. CNCs with different coil diameters and structures could be selectively synthesized by optimizing the thickness of the catalyst film. The mechanism governing the growth of CNCs by Sn/Fe catalyst films was also investigated.

2. Experimental

Sn–Fe binary metals were used as the catalyst precursors for synthesizing CNCs. To prepare the Sn/Fe catalyst precursors, a tin film was first sputtered on a silicon substrate (size: $1 \times 1\ cm^2$) by a vacuum magnetron sputtering system (JCP-200, BTSC563). Then, an iron film was sputtered onto the tin film. The thickness ratio of Sn to Fe was maintained at 1:20, and the mole ratio of Sn to Fe was approximately 1:46. A series of Sn/Fe films with thicknesses ranging from 0.035/0.7 to 16/320 nm was prepared. The prepared Sn/Fe catalyst films were then calcined at 710 °C for 30 min in the air to oxidize the catalysts, which prevents Sn from vaporization during heating in Ar, because the melting point of Sn is 231.89 °C [20]. Finally, CNCs were synthesized in a thermal CVD system at 710 °C by introducing Ar and C_2H_2 at flow rates of 230 and 30 sccm, respectively.

The morphology and structure of the synthesized CNCs were analyzed by scanning electron microscopy (SEM; FEI, NOVA NanoSEM 450), transmission electron microscopy (TEM; FEI, Tecnai G2 F30 S-Twin), and Raman spectroscopy (Renishaw inVia plus, He-Ne laser, 632.8 nm). The Sn/Fe catalyst films were characterized by atomic force microscopy (AFM; Agilent PicoPlus II, Agilent, Santa Clara, CA) and SEM.

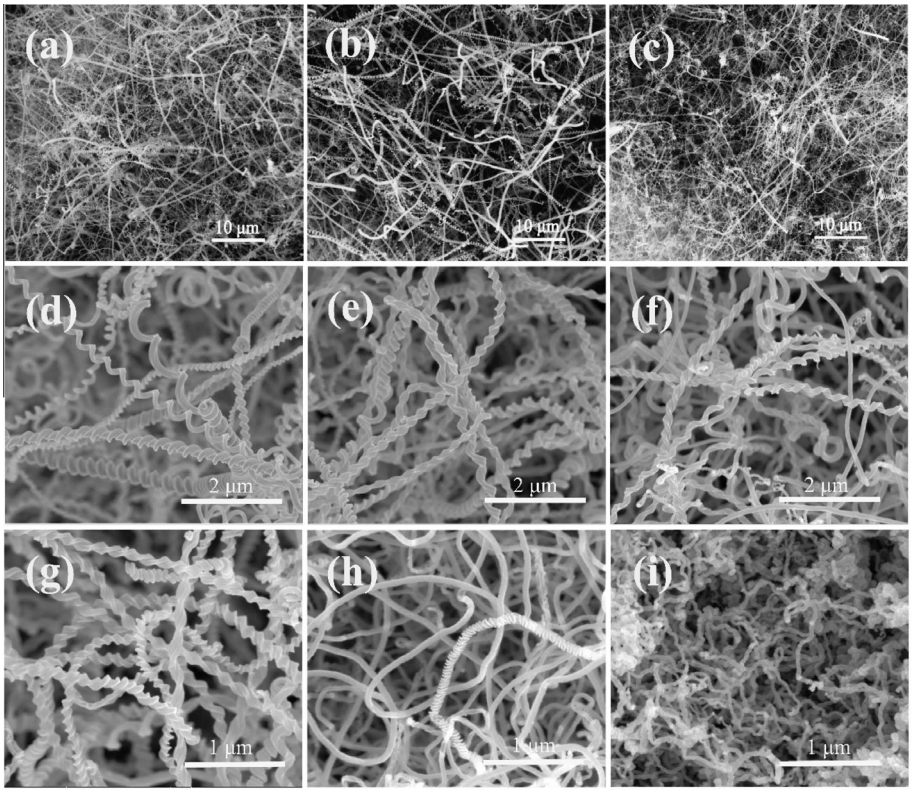

Fig. 1 – SEM images of carbon deposits synthesized using Sn/Fe catalyst films with different thicknesses of, (a) 16/320 nm, (b) 8/160 nm, (c) 4/80 nm, (d) 2/40 nm, (e) 1/20 nm, (f) 0.5/10 nm, (g) 0.35/7 nm, (h) 0.15/3 nm, and (i) 0.035/0.7 nm.

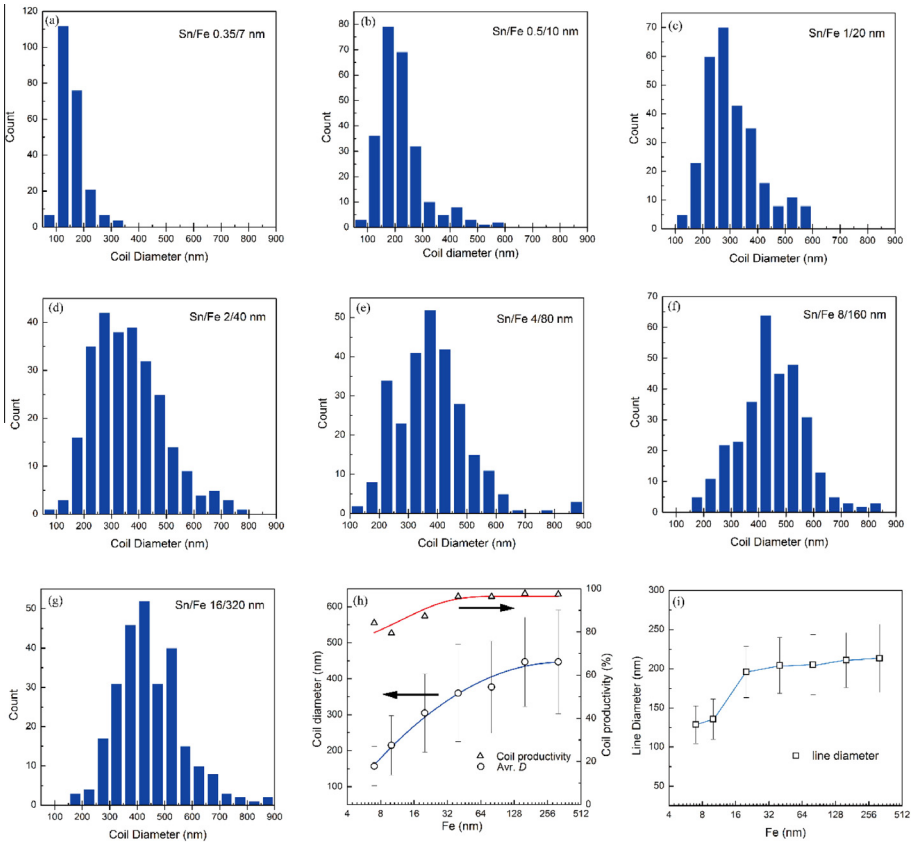

Fig. 2 – Statistical distribution of coil diameters of the CNCs synthesized using Sn/Fe catalyst films with different thicknesses of, (a) 0.35/7 nm, (b) 0.5/10 nm, (c) 1/20 nm, (d) 2/40 nm, (e) 4/80 nm, (f) 8/160 nm, and (g) 16/320 nm. (h) Systematic statistics of the average coil diameter and productivity of the CNCs on the surface changing with the thickness of catalyst films. (i) Systematics statistics of the average line diameter of the CNCs changing with the thickness of catalysts films. (A color version of this figure can be viewed online.)

3. Results and discussion

Fig. 1 shows typical SEM images of carbon deposits synthesized using Sn/Fe catalyst films with thicknesses of (a) 16/320 nm, (b) 8/160 nm, (c) 4/80 nm, (d) 2/40 nm, (e) 1/20 nm, (f) 0.5/10 nm, (g) 0.35/7 nm, (h) 0.15/3 nm, and (i) 0.035/0.7 nm. It is observed that CNCs, carbon nanofibers (CNFs), and irregular carbon nanowires (irregular CNWs) are selectively obtained by using Sn/Fe catalyst films with different thicknesses. CNCs are synthetized by using Sn/Fe catalyst films with the wide range of thicknesses, i.e., 16/320, 8/160, 4/80, 2/40, 1/20, 0.5/10, and 0.35/7 nm as shown in Fig. 1(a–g). And the coil diameter of the CNCs is reduced by decreasing the thickness of the catalyst film. When the thickness of the catalyst film is reduced to 0.15/3 nm, CNFs and only a few CNCs are synthesized, as shown in Fig. 1(h). Irregular CNWs are obtained by using a 0.035/0.7 nm Sn/Fe catalyst film, as shown in Fig. 1(i). A comparison of Fig. 1(h) with (i) reveals that the average diameters of the CNFs and irregular CNWs are also reduced by decreasing the thickness of the Sn/Fe catalyst film. These results indicate that the minimum catalyst film required thickness for the efficient synthesis of CNCs is 3–7 nm.

The distribution of coil diameter of the CNCs synthesized by using Sn/Fe catalyst films with different thickness were analyzed statistically, as shown in Fig. 2(a–g). It is found that the distribution center of coil diameter shifts to large value with increasing the thickness of catalyst film. When the thickness of the catalyst film is larger than 8/160 nm, the distributions of coil diameter have little change. The average coil diameter and the productivity of the apparent CNCs synthesized by using Sn/Fe catalyst films with different thicknesses were analyzed statistically, as shown in Fig. 2(h). It is observed that the coil diameters of the CNCs obtained by using 16/320 and 8/160 nm Sn/Fe catalyst films are both approximately 450 nm, indicating that the sizes and distributions of the catalyst particles in the two samples are similar. The average coil diameter of the CNCs is reduced by decreasing the thickness of catalyst film. When the thickness of the Sn/Fe catalyst film is decreased from 8/160 to 0.35/7 nm, the average coil diameter of the CNCs is reduced from 450 to 150 nm. The productivity of the apparent CNCs remains stable at approximately 97%, when the Sn/Fe catalyst film is thicker than 2/40 nm. The coil productivity begin to decrease when the thickness of the catalyst film is thinner than 2/40 nm.

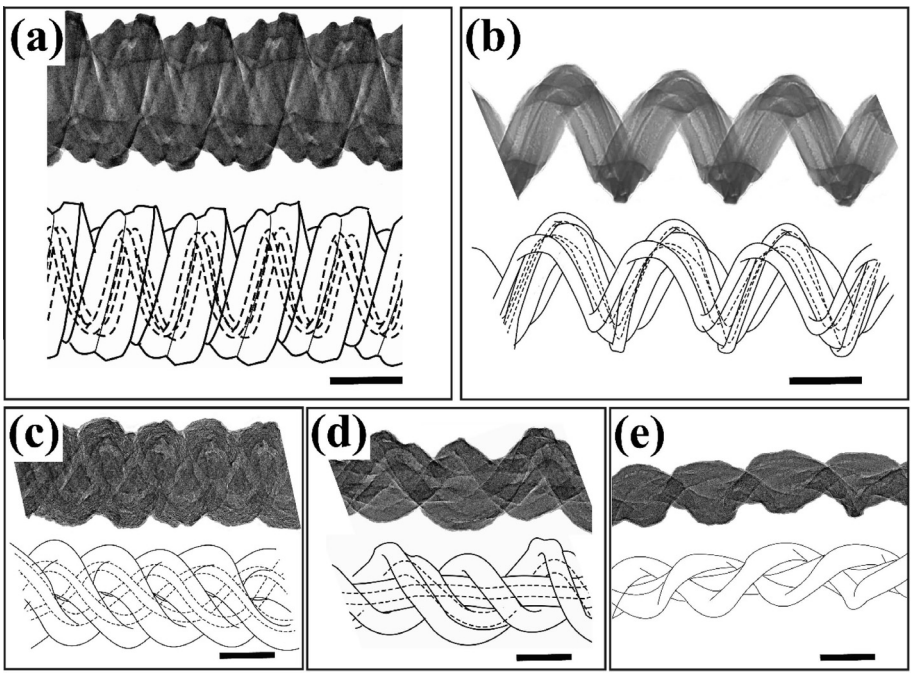

Fig. 3 – TEM images and schematic illustrations of CNCs. (a) A CNC formed by two tubules with nearly the same pitch and phase. (b) A CNC formed by three tubules with nearly the same pitch and phase. (c) A CNC formed by three tubules with near the same pitch and different phases. (d) A CNC formed by two tubules and a fiber. (e) A CNC formed by two fibers with different phases. The scale bar for (a) and (b) is 200 nm, and the scale bar for (c–e) is 100 nm.

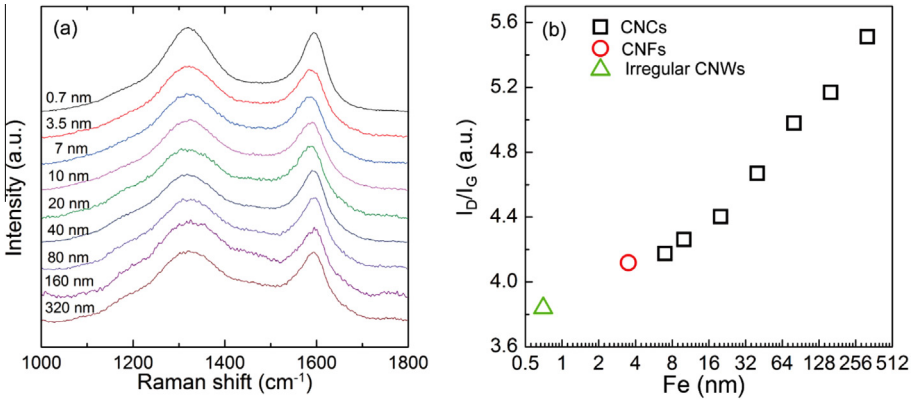

Fig. 4 – (a) Raman spectra of the carbon products generated using Sn/Fe catalyst films with different thicknesses. The data in the figure denote the series of Fe film thicknesses. (b) The relationship between the thickness of the Fe film and the ratio I_D/I_G for the corresponding carbon deposits. (A color version of this figure can be viewed online.)

Hokushin and Pan et al. found that the line diameter of a CNC is determined by the size of the catalyst particle at the tip of the CNC and the coil diameter of a CNC is proportional to the size of the catalyst particle [27]. So the catalyst particles have similar distribution with the line diameter of the grown CNCs. Fig. 2(i) shows the average line diameter of the CNCs synthesized by using Sn/Fe catalyst films with different thickness, revealing that the average line diameter of the CNCs is reduced by decreasing the thickness of catalyst film. Fig. 2(h) and (i) further reveals that the line diameter of the CNCs is proportional to the coil diameter of the CNC. All these results suggest that the size of catalyst particle of the CNC is reduced by decreasing the thickness of catalyst film.

The structures of the synthesized CNCs were analyzed by TEM and Raman spectroscopy. Fig. 3 shows the TEM images and schematic illustrations of the typical CNCs obtained with different coil diameters. The TEM images reveal that the CNCs consisted of carbon tubules and carbon fibers. In most cases, the CNCs are formed by at least two tubules or fibers. The morphology and structure of the CNCs are determined by the correlation between the tubules or the fibers. It is observed that the morphology and structure of the CNCs changed with the coil diameter. Fig. 3(a) and (b) shows the typical structures of CNCs with a coil diameter larger than 200 nm. The CNC consists of two spiral tubules with the same pitch and phase as shown in Fig. 3(a). A similar spring-like

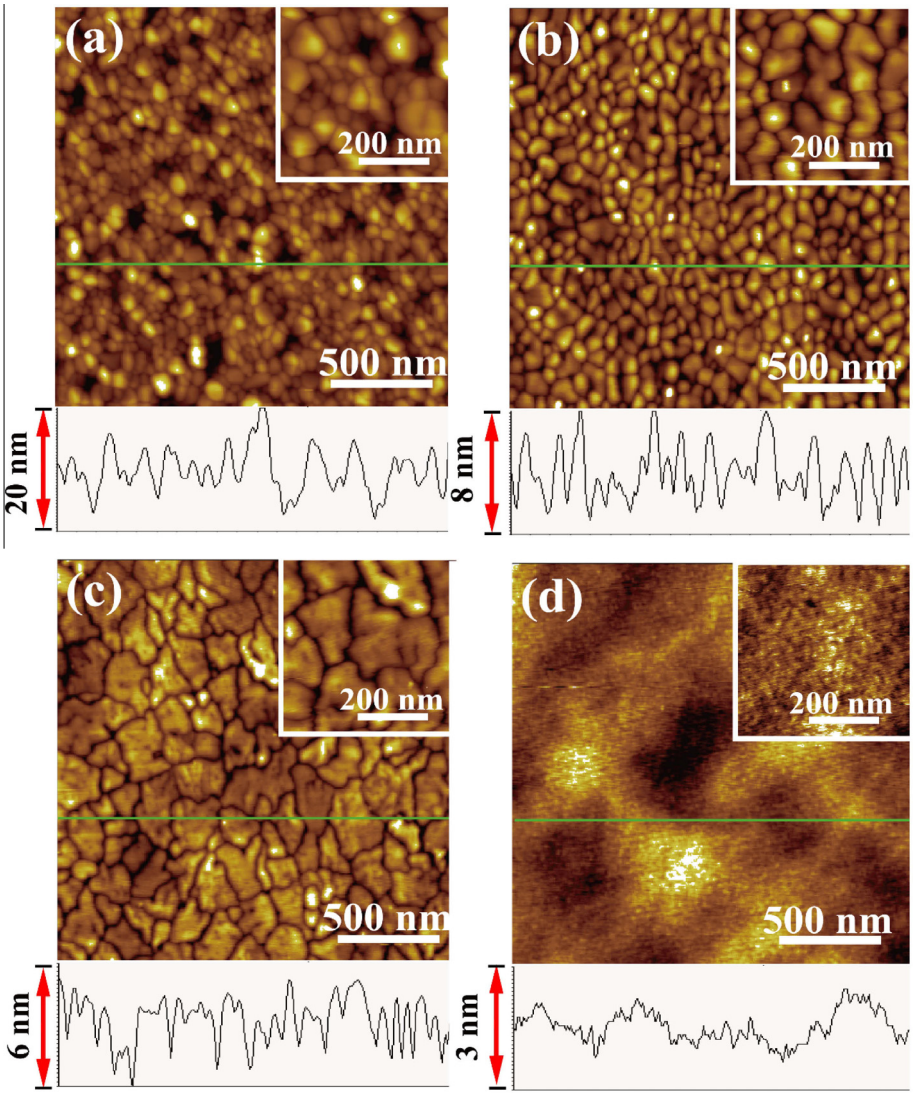

Fig. 5 – AFM images of samples with original catalyst film thicknesses of (a) 2/40 nm, (b) 0.35/7 nm, (c) 0.15/3 nm, and (d) 0.035/0.7 nm after calcination at 710 °C for 30 min in air. The corresponding cross-sectional height along the line is shown below each topograph. The insets show the corresponding enlarged images. (A color version of this figure can be viewed online.)

CNC consisting of three spiral tubules with the same pitch and phase is shown in Fig. 3(b). Fig. 3(c–e) shows the typical structures of CNCs with a coil diameter smaller than 200 nm. The CNC illustrated in Fig. 3(c) is composed of three tubules with uniform pitch and different phases. The CNC in Fig. 3(d) comprises a fiber and a tubule, both of which are twisted around a straight tubule with different phases. Similarly, Fig. 3(e) represents a CNC composed of two fibers with different phases. Further statistical study reveals that the structure of the CNC changed with the coil diameter of the CNC. When the coil diameter of the CNC is larger than 200 nm, the tubules or fibers in most of the CNCs possess the same phase. For the coil diameters smaller than 200 nm, the tubules or fibers in most of the CNCs have different phases. From a morphological point of view, the CNCs tend to change from spring-like to plait-like as their diameters are decreased. The results from the observation of TEM and SEM, as well as Fig. 2(i) reveal that 0.5/10 nm Sn/Fe catalyst film is a kink-point for the CNCs changing from spring-like to plait-like.

CNCs obtained by using catalyst films with different thicknesses were inspected by Raman spectroscopy at an excitation wavelength of 632.8 nm, as shown in Fig. 4. Two main peaks are observed in the Raman spectra: one at approximately 1322 cm^{-1}, known as the D-band, which originates from structural defects in carbon materials, and the other at approximately 1593 cm^{-1}, known as the G-band, which originates from the graphitic structure of carbon materials (Fig. 4(a)). The Lorentz and Breit–Wigner–Fano (BWF) function are used to peak fit the D-band and G-band, respectively [28]. The area ratio of the D-band to the G-band is denoted as I_D/I_G. As the thicknesses of the Sn/Fe catalyst films is reduced from 16/320 to 0.035/0.7 nm, the value of I_D/I_G for the corresponding carbon deposits decrease from 5.5 to 3.8, indicating that the

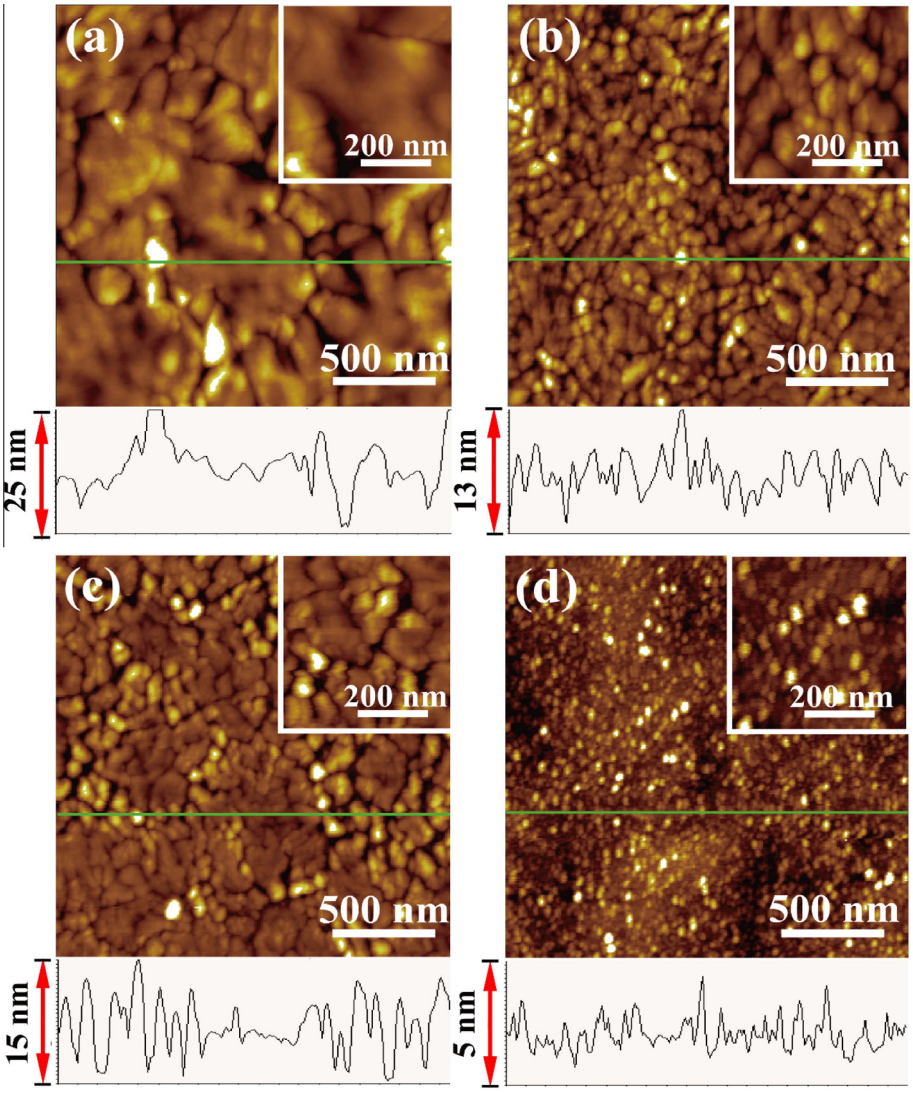

Fig. 6 – AFM images of samples with original catalyst film thicknesses of (a) 2/40 nm, (b) 0.35/7 nm, (c) 0.15/3 nm, and (d) 0.035/0.7 nm after feeding acetylene with a flow rate of 2 sccm at 710 °C for 2 s. The corresponding cross-sectional height along the line is shown below each topograph. The insets show the corresponding enlarged images. (A color version of this figure can be viewed online.)

irregular CNWs possess a more graphitic structure than do the CNFs and CNCs. In addition, the value of I_D/I_G for the CNCs decrease with the decrease in the coil diameters of the CNCs. Fig. 4(a) further reveals that the G peaks are red shifted with the decrease in the thickness of the Sn/Fe catalyst films, indicating that the carbon products obtained gradually change from having an amorphous carbon structure to having a nanocrystalline graphite structure [28].

Why dose the thickness of the catalyst films affect the morphology and structure of the obtained carbon products so strongly? To study the mechanism of synthesizing CNCs by using Sn/Fe catalyst films with different thicknesses, the catalyst particles were further investigated by AFM and SEM. Fig. 5 shows AFM images of the samples with the original catalyst film thicknesses of (a) 2/40 nm, (b) 0.35/7 nm, (c) 0.15/3 nm, and (d) 0.035/0.7 nm after calcination at 710 °C for 30 min in the air. It is observed that the height differences decreased with the decrease in the thicknesses of the Sn/Fe catalyst films. The height difference for the sample with 2/40 nm Sn/Fe catalyst film is approximately 15 nm which is smaller than the original thickness of the catalyst film as shown in Fig. 5(a). This discrepancy is observed because several layers of catalyst particles are piled up to form the film. However, the height differences for the samples with 0.35/7, 0.15/3, and 0.035/0.7 nm Sn/Fe catalyst films are approximately 7, 3, and 0.7 nm, respectively. The height difference for these samples are similar with their original thickness of catalyst film, indicating that there is only one layer of catalyst particles on each substrate as shown in Fig. 5(b–d).

Fig. 6 shows AFM images of the samples obtained after feeding acetylene with a flow rate of 2 sccm at 710 °C for 2 s. A comparison of Fig. 5(a) with Fig. 6(a) shows that the catalyst particles aggregated into larger particles for the 2/40 nm Sn/Fe catalyst film after feeding acetylene. For the 0.35/7 nm Sn/Fe catalyst film after feeding acetylene, the catalyst particles also aggregated into larger particles as shown in

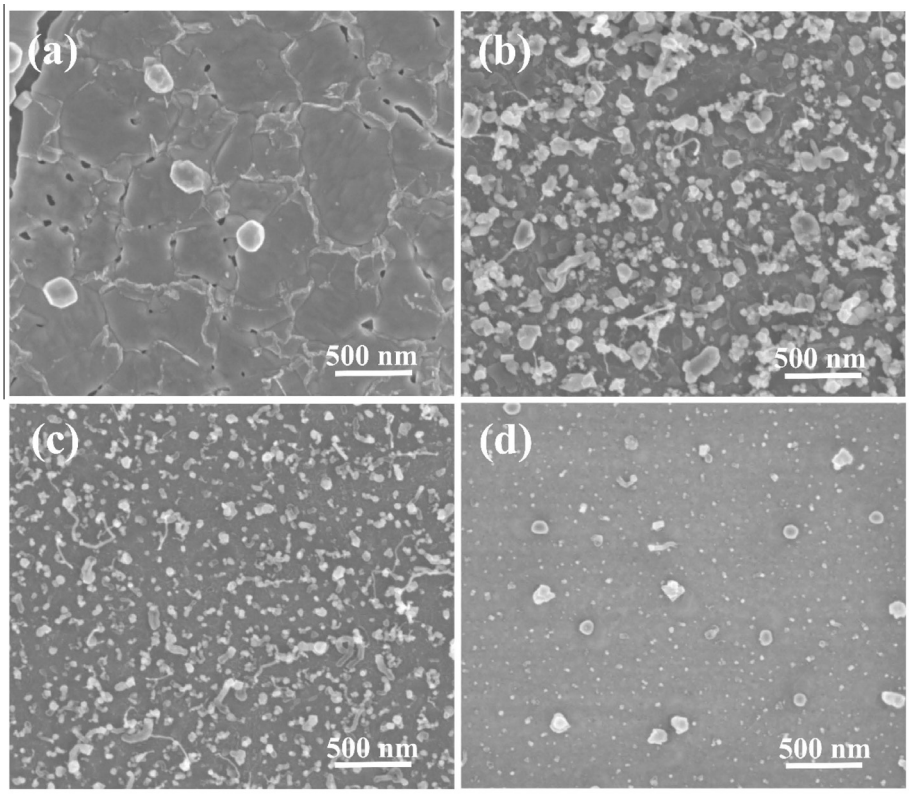

Fig. 7 – SEM images of samples with original catalyst film thicknesses of (a) 2/40 nm, (b) 0.35/7 nm, (c) 0.15/3 nm, and (d) 0.035/0.7 nm after feeding acetylene with a flow rate of 2 sccm at 710 °C for 10 s.

Figs. 5(b) and 6(b). However, the Sn/Fe catalyst film with a thickness of 0.15/3 nm is split into small particles, among which only a few tended to form aggregates on the surface of the substrate, as shown in Figs. 5(c) and 6(c). Furthermore, Figs. 5(d) and 6(d) show that the continuous catalyst film is broke down into discrete small catalyst particles. Figs. 5 and 6 further reveal that the morphology of the Sn/Fe catalyst tend to change from particle-like to film-like after being oxidized when their thicknesses are reduced, whereas the situation is precisely the opposite after feeding acetylene. All of the changes observed for the catalyst particles are attributed to the reduction and carbonization of the particles and the subsequent carbon precipitation of these particles [29,30]. The height differences of the samples increased after feeding acetylene due to the carbon precipitation.

Fig. 7 shows SEM images of samples with original catalyst film thicknesses of (a) 2/40 nm, (b) 0.35/7 nm, (c) 0.15/3 nm, and (d) 0.035/0.7 nm after feeding acetylene at 2 sccm for 10 s at 710 °C. It can be observed that many aggregates of catalyst particles are obtained, the sizes of which increased with the thickness of the catalyst film. Certain carbon nanofibers or germinations of CNCs are grown from the surface of the aggregations as shown in Fig. 7(b–d). However, no carbon nano-materials are observed in Fig. 7(a). This latter result can be attributed to the fact that the amount of the carbon source is too little to complete the carbon precipitation process.

It is accepted from mechanics viewpoint that the spiral motion of a CNC during its growth should generate a torsional moment on its base [31,32]. Therefore, base fixation is a crucial condition for the growth of CNCs [33]. Generally, there are two kinds of catalyst particles formed in the CVD process. One is for the growth of CNCs, CNFs, and irregular CNWs. The other one is not suitable for the growth of these nanomaterials but contributes to form a compact aggregation by carbon precipitation that fixes the base of a grown CNC. When a catalyst film is too thin, the formed catalyst particles are discrete, which cannot form a sufficient aggregation to afford the base-fixation for the growth of a CNC. Therefore, only CNFs or Irregular CNWs are grown from these discrete catalyst particles. Further observation of Fig. 7(a) reveals that the catalyst particles almost aggregate into a continuous film for the 2/40 nm Sn/Fe catalyst film, which would provide strong base fixation. Many aggregates of catalyst particles are observed to form and the aggregates are large for the 0.35/7 nm Sn/Fe catalyst film, which can afford the appropriate base fixation for growing CNCs, as shown in Fig. 7(b). As the thickness of the Sn/Fe catalyst film is decreased to 0.15/3 nm, only a few catalyst particles aggregate, but the aggregates are too small to afford the appropriate base fixation for the growth of CNCs, which result in low coil productivity. For the 0.035/0.7 nm Sn/Fe catalyst film, the catalyst particles are discrete, and only irregular CNWs are synthesized. This result is in agreement with our AFM and CVD results.

Hirahara et al. have report that significant amount of tin vaporized for preparing optimized catalytic particles at the initial stage of CVD [34]. In our experiment, the amount of tin is reduced with decreasing the thickness of Sn/Fe catalyst film. Therefore, the amount of vaporized tin is reduced with decreasing the thickness of Sn/Fe catalyst film. This would be one of the reasons for the decrease of coil productivity in the circumstance of thinner catalyst films.

In fact, the changes in morphology, structure and productivity of CNCs with the decrease of catalyst film are fundamentally due to the changes of catalyst particles. The changes in structure and composition of catalyst particles in the CVD process are very complex, which is an important subject for our future study.

4. Conclusion

CNCs with different coil diameters and structures could be selectively synthesized with great control by optimizing the thickness of the catalyst film prepared by vacuum magnetron sputtering. The average coil diameter is increased from 150 to 450 nm by increasing the thickness of the Sn/Fe catalyst film from 0.35/7 to 16/320 nm. CNFs and irregular CNWs can also be synthesized by using 0.15/3 and 0.035/0.7 nm Sn/Fe catalyst films, respectively. The morphology of the CNCs tends to change from spring-like to plait-like and the graphitization degree of the CNCs increases as the thickness of catalyst film is reduced. The minimum catalyst film thickness for growing CNCs in a high yield is determined to be approximately 3–7 nm. All conditions mentioned above provide significant control for synthesizing CNCs with selective coil diameters and structures.

Acknowledgements

This work was supported by the National Natural Science Foundation of China (Nos. 11274055 and 61137005) and the Program for Liaoning Excellent Talents in University.

REFERENCES

[1] Hayashida T, Pan LJ, Nakayama Y. Mechanical and electrical properties of carbon tubule nanocoils. Physica B 2002;323(1–4):352–3.
[2] Treacy MMJ, Ebbesen TW, Gibson JM. Exceptionally high Young's modulus observed for individual carbon nanotubes. Nature 1996;381(6584):678–80.
[3] Ma H, Pan LJ, Zhao Q, Peng W. Near-infrared response of a single carbon nanocoil. Nanoscale 2013;5(3):1153–8.
[4] Ma H, Pan LJ, Zhao Q, Zhao ZB, Qiu JS. Thermal conductivity of a single carbon nanocoil measured by field-emission induced thermal radiation. Carbon 2012;50(3):778–83.
[5] Ma H, Pan LJ, Zhao Q, Zhao ZB, Zhao JZ, Qiu JS. Electrically driven light emission from a single suspended carbon nanocoil. Carbon 2012;50(15):5537–42.
[6] Li LL, Pan LJ, Li DW, Zhao Q, Ma H. Field emission properties of carbon nanocoils synthesized on stainless steel. New Carbon Mater 2014;29(1):34–40.
[7] Motojima S, Noda Y, Hoshiya S, Hishikawa Y. Electromagnetic wave absorption property of carbon microcoils in 12–110 GHz region. J Appl Phys 2003;94(4):2325–30.
[8] Yang SM, Chen XQ, Motojima S. Tactile sensing properties of protein-like single-helix carbon microcoils. Carbon 2006;44(15):3352–5.
[9] Pan LJ, Hayashida T, Zhang M, Nakayama Y. Field emission properties of carbon tubule nanocoils. Jpn J Appl Physcs Part 2 Lett 2001;40(3B):L235–L7.
[10] Sato S, Pan LJ, Nakayama Y, Akita S. Resonant vibration of cantilevered carbon nanocoil. Microprocesses Nanotechnol 2007, Digest of Papers 2007:468–9.
[11] Chen XQ, Zhang SL, Dikin DA, Ding WQ, Ruoff RS, Pan LJ, et al. Mechanics of a carbon nanocoil. Nano Lett 2003;3(9):1299–304.
[12] Zhao Q, Pan LJ, Ma H, Wang T. Structure changes of an individual carbon nanocoil and its field-emission enhancement by laser treatment. Diam Relat Mater 2012;22:33–6.
[13] Deng C, Pan LJ, Ma H, Cui R. Electromechanical vibration of carbon nanocoils. Carbon 2015;81:758–66.
[14] Ma H, Nakata K, Pan LJ, Hirahara K, Nakayama Y. Relationship between the structure of carbon nanocoils and their electrical property. Carbon 2014;73:71–7.
[15] Pan LJ, Konishi O, Tanaka H, Suekane O, Nosaka T, Nakayama Y. Effect of morphology on field emission properties of carbon nanocoils and carbon nanotubes. Jpn J Appl Phys 1 2005;44(4A):1652–4.
[16] Pan LJ, Hayashida T, Harada A, Nakayama Y. Effects of iron and indium tin oxide on the growth of carbon tubule nanocoils. Physica B 2002;323(1–4):350–1.
[17] Jian XA, Jiang M, Zhou ZW, Yang ML, Lu J, Hu SC, et al. Preparation of high purity helical carbon nanofibers by the catalytic decomposition of acetylene and their growth mechanism. Carbon 2010;48(15):4535–41.
[18] Li DW, Pan LJ, Liu K, Peng W, Muhammad R. Growth of multiwall carbon nanocoils using Fe catalyst films prepared by ion sputtering (vol 28, p. 1316, 2013). J Mater Res 2013;28(14):1972–5.
[19] Nitze F, Abou-Hamad E, Wågberg T. Carbon nanotubes and helical carbon nanofibers grown by chemical vapour deposition on C_{60} fullerene supported Pd nanoparticles. Carbon 2011;49(4):1101–7.
[20] Kanada R, Pan LJ, Akita S, Okazaki N, Hirahara K, Nakayama Y. Synthesis of multiwalled carbon nanocoils using codeposited thin film of Fe–Sn as catalyst. Jpn J Appl Phys 2008;47(4R):1949.
[21] Chang NK, Chang SH. High-yield synthesis of carbon nanocoils on stainless steel. Carbon 2008;46(7):1106–9.
[22] Li DW, Pan LJ, Qian JJ, Liu DP. Highly efficient synthesis of carbon nanocoils by catalyst particles prepared by a sol–gel method. Carbon 2010;48(1):170–5.
[23] Zheng GB, Kouda K, Sano H, Uchiyama Y, Shi YF, Quan HJ. A model for the structure and growth of carbon nanofibers synthesized by the CVD method using nickel as a catalyst. Carbon 2004;42(3):635–40.
[24] Liu Q, Cui ZM, Ma Z, Bian SW, Song WG. Carbon materials with unusual morphologies and their formation mechanism. J Phys Chem C 2007;111(33):12420–4.
[25] Li DW, Pan LJ, Wu YK, Peng W. The effect of changes in synthesis temperature and acetylene supply on the morphology of carbon nanocoils. Carbon 2012;50(7):2571–80.
[26] Fu X, Li DW, Pan LJ. Investigation on Fe–Sn–O catalyst activity for the growth of carbon nanocoils. Appl Mech Mater 2013;420:154–9.
[27] Hokushin S, Pan LJ, Nakayama Y. Diameter control of carbon nanocoils by the catalyst of organic metals. Jpn J Appl Phys 1 2007;46(8A):5383–5.

[28] Ferrari AC, Robertson J. Interpretation of Raman spectra of disordered and amorphous carbon. Phys Rev B 2000;61(20):14095–107.
[29] Nishimura K, Okazaki N, Pan LJ, Nakayama Y. In situ study of iron catalysts for carbon nanotube growth using X-ray diffraction analysis. Jpn J Appl Phys 2 2004;43(4A):L471–L4.
[30] Qian JJ, Pan LJ, Li DW, Yu NS, Liu DP. Formation of catalyst particles for carbon nanocoil growth. J Nanosci Nanotechnol 2010;10(11):7366–9.
[31] Motojima S, Chen QQ. Three-dimensional growth mechanism of cosmo-mimetic carbon microcoils obtained by chemical vapor deposition. J Appl Phys 1999;85(7):3919–21.
[32] Li DW, Pan LJ, Liu DP, Yu NS. Relationship between geometric structures of catalyst particles and growth of carbon nanocoils. Chem Vapor Deposition 2010;16(4–6):166–9.
[33] Li DW, Pan LJ. Necessity of base fixation for helical growth of carbon nanocoils. J Mater Res 2012;27(2):431–9.
[34] Hirahara K, Nakayama Y. The effect of a tin oxide buffer layer for the high yield synthesis of carbon nanocoils. Carbon 2013;56:264–70.